Auxin-Dependent Patterning and Gamete Specification in the *Arabidopsis* Female Gametophyte

Gabriela C. Pagnussat,[1]* Monica Alandete-Saez,[1] John L. Bowman,[1,2] Venkatesan Sundaresan[1,3]†

The female reproductive unit of flowering plants, the haploid female gametophyte, is highly reduced relative to other land plants. We show that patterning of the *Arabidopsis* female gametophyte depends on an asymmetric distribution of the hormone auxin during its syncitial development. Furthermore, this auxin gradient is correlated with location-specific auxin biosynthesis, rather than auxin efflux that directs patterning in the diploid sporophytic tissues comprising the rest of the plant. Manipulation of auxin responses or synthesis induces switching of gametic and nongametic cell identities and specialized nonreproductive cells to exhibit attributes presumptively lost during angiosperm evolution. These findings may account for the unique egg cell specification characteristic of angiosperms and the formation of seeds with single diploid embryos while containing endosperm that can have variable numbers of parental haploid genomes.

The highly reduced female gametophyte of flowering plants (*1, 2*), with specialized gametes to enable double fertilization, constitutes a microcosm of pattern formation and gamete specification for which the underlying mechanisms have remained elusive (*3–7*). In *Arabidopsis* and most other flowering plants, the female gametophyte, referred to as the embryo sac, first develops as a syncitium, a structure that contains eight nuclei, which are later partitioned into seven cells consisting of four cell types. These are the egg cell and central cell that form the gametes for double fertilization, two accessory synergid cells positioned next to the egg cell, and three antipodal cells. Manifestation of cell identity is concomitant with cellularization, suggesting that cell fates are programmed before this stage. Moreover, it has been shown that unusual positioning of the nuclei during embryo sac de-

velopment, as observed in the *eostre* mutant, can lead to both morphological and functional defects, including the production of an extra functional egg cell in place of a synergid (*8*). These observations suggested that, in angiosperms, the determination of egg cell fate may depend on a location-specific mechanism within the syncitial female gametophyte. Additional support for this conjecture comes from observations of the maize *indeterminate gametophyte* mutant in which extra cells are generated that appear to assume specific cell fates correlated with their position (*9*). On the basis of these findings, we hypothesize that positional information within the syncitium might rely on the asymmetric distribution of a morphogenetic determinant as described in animals such as the development of the *Drosophila* embryo (*10*).
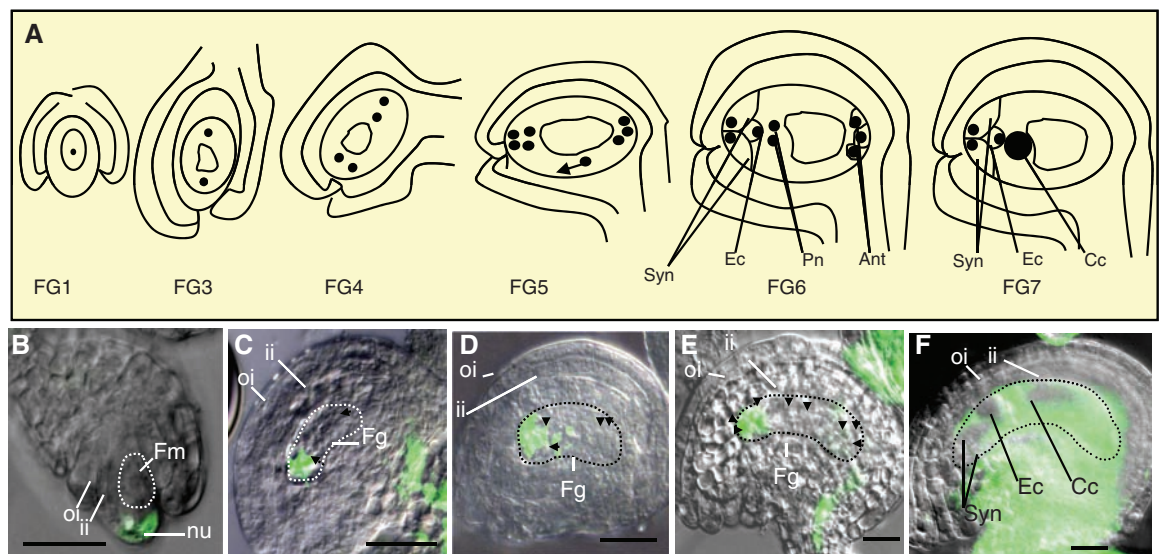
Auxin, auxin response, and cell specification. The phytohormone auxin regulates cell division, elongation, and differentiation in plants. Local accumulation of auxin provides positional signals for multiple developmental processes, such as establishment of the shoot and root meristems along the apical-basal axis, organogenesis, and vascular differentiation (*11–14*). In order to determine whether auxin acts as a positional determinant regulating cell specification during megagametogenesis in *Arabidopsis*, we followed the distribution of auxin by DR5-driven expression in the synthetic reporters *DR5::GFP* and *DR5::GUS* (GFP is green fluorescent protein, and GUS is β-glucuronidase) (*14, 15*). Auxin signaling output was traced to megasporogenesis, the stage at which a signal was detectable at the distal tip of the nucellus (fig. S1A). At gametophyte developmental stage FG1, when a functional megaspore is visible, the signal is strong in the nucellus, outside the

[1]Department of Plant Biology, University of California, Davis, CA 95616, USA. [2]School of Biological Sciences, Monash University, Melbourne, Victoria 3800, Australia. [3]Department of Plant Sciences, University of California, Davis, CA 95616, USA.

*Present address: Instituto de Investigaciones Biológicas, Universidad Nacional de Mar del Plata, 7600 Mar del Plata, Argentina.

†To whom correspondence should be addressed. E-mail: sundar@ucdavis.edu

Fig. 1. Expression of the synthetic reporters *DR5::GFP* during female gametophyte development. (**A**) Scheme showing the developmental stages during wild-type female gametophyte development in *Arabidopsis*. Ant indicates antipodal cells; Cc, central cell; Ec, egg cell; Fg, female gametophyte; Fm, functional megaspore; ii, inner integument; nu, nucellus; oi, outer integument; Pn, polar nuclei; and Syn, synergid. (**B**), At FG1, the signal is strongly detected in the nucellus, outside the embryo sac. Scale bar indicates 25 μm, and the developing embryo sac is delimited by a dashed line. (**C**) At FG3 stage, the signal is detectable inside the embryo sac at the micropylar pole. (**D**) As the female gametophyte continues to develop, a strong *DR5::GFP* signal is localized to the micropylar end of the embryo sac by stage FG4. Small black arrowheads indicate nuclei inside the developing embryo sac. (**E**) A *DR5::GFP* activity maximum at the micropylar end of the embryo sac could be detected up to FG5 stage. (**F**) At FG6 stage the distribution of the *DR5::GFP* signal becomes less polarized. Signals outside the developing embryo sac in (C), (E), and (F) correspond to vascular tissues in the sporophytic ovule, particularly the funiculus.

developing embryo sac (Fig. 1, A and B, and fig. S1B). At the FG3 stage, after the first mitotic division and when the two resulting nuclei are separated by a small vacuole, the signal is detectable at the micropylar pole inside the embryo sac where one of the two nuclei is located (Fig. 1, A and C, and fig. S1C). As the female gametophyte developed, a strong signal was localized to the micropylar end of the developing embryo sac by stage FG4, after the second mitotic di-

vision, with one pair of nuclei located at the chalazal end of the gametophyte and the other pair at the micropylar end (Fig. 1, A and D). The *DR5::GFP* activity maximum at the micropylar end of the female gametophyte could be detected up to the FG5 stage, in which the third mitotic division was completed and eight nuclei were localized along the gametophyte (Fig. 1, A and E). These observations suggest that an auxin maximum is formed at the micropylar pole of the de-

veloping embryo sac. At late stages, that is, after cellularization, the distribution of the *DR5::GFP* signal appeared less polarized than in earlier stages and was detectable in all cells of the mature embryo sac (stage FG6, Fig. 1, A and F).

To determine whether the auxin maximum observed in the developing syncitial embryo sac conveys positional information for cell specification, we down-regulated genes involved in the auxin response with an artificial microRNA (miRNA) called *amiR-ARFa* targeting a subset of the auxin response factor genes (*ARFs*), a family of transcriptional regulator proteins that mediate responses to auxin by using a sequence highly conserved in ARFs from two major clades (fig. S5). Because many ARFs have essential functions in sporophyte development, we constructed transgenic plants carrying a pOp/LhG4 system to restrict the expression of *amiR-ARFa* to the embryo sac (*16*). This system was driven by the embryo sac promoter *pES1* (*8*), which is uniformly expressed during early female gametophyte development (stage FG1) to the mature embryo sac (stage FG7). To confirm that expression of *amiR-ARFa* by *pES1* results in down-regulation of the auxin response in the embryo sac, these transgenic plants were crossed to plants carrying the DR5::GFP auxin reporter. By scoring for DR5::GFP expression in the unfertilized pistils of the progeny, we showed that GFP-expressing embryo sacs were reduced by the predicted fraction, indicating down-regulation of the auxin response by *amiR-ARFa* (fig. S2 and table S1).

We observed that *ARF* down-regulation resulted in F1 plants with defective embryo sacs at ratios close to the expected 0.25 for co-inheritance of the driver and miRNA transgenes (table S2). Examination of the lines showing the greatest penetrance of the miRNA constructs revealed that defective embryo sacs developed to maturity but were unfertilized. Differential interference contrast (DIC) microscopy of mature defective embryo sacs revealed that the three cells at the micropylar end had identity defects (i.e., could not be recognized as egg cells or synergids) or had more than one cell exhibiting features characteristics of an egg cell (i.e., nucleus toward the chalazal end of the embryo sac and a large vacuole toward the micropylar end of the embryo sac) (Fig. 2, A to D).

We introduced cell-type specific GUS markers into the *pES* driven *amiR-ARFa* background to further examine cell identity. We observed that, although two micropylar cells were GUS positive for the expression of a synergid-specific marker [ET884 (*6*)] in wild-type embryo sacs, this marker was not detected in abnormal embryo sacs (fig. S2, A and B, and table S3). Concordantly, none of the mutant embryo sacs attracted pollen tubes, which is consistent with the loss of synergid cell identity (fig. S3E). For the egg cell–specific marker [ET119 (*6*)], we could detect expression of the marker in all three micropylar for 10 out of 489 embryo sacs examined (where 61 embryo sacs are expected to inherit all three transgenes; table S3), suggesting that synergid identity had been
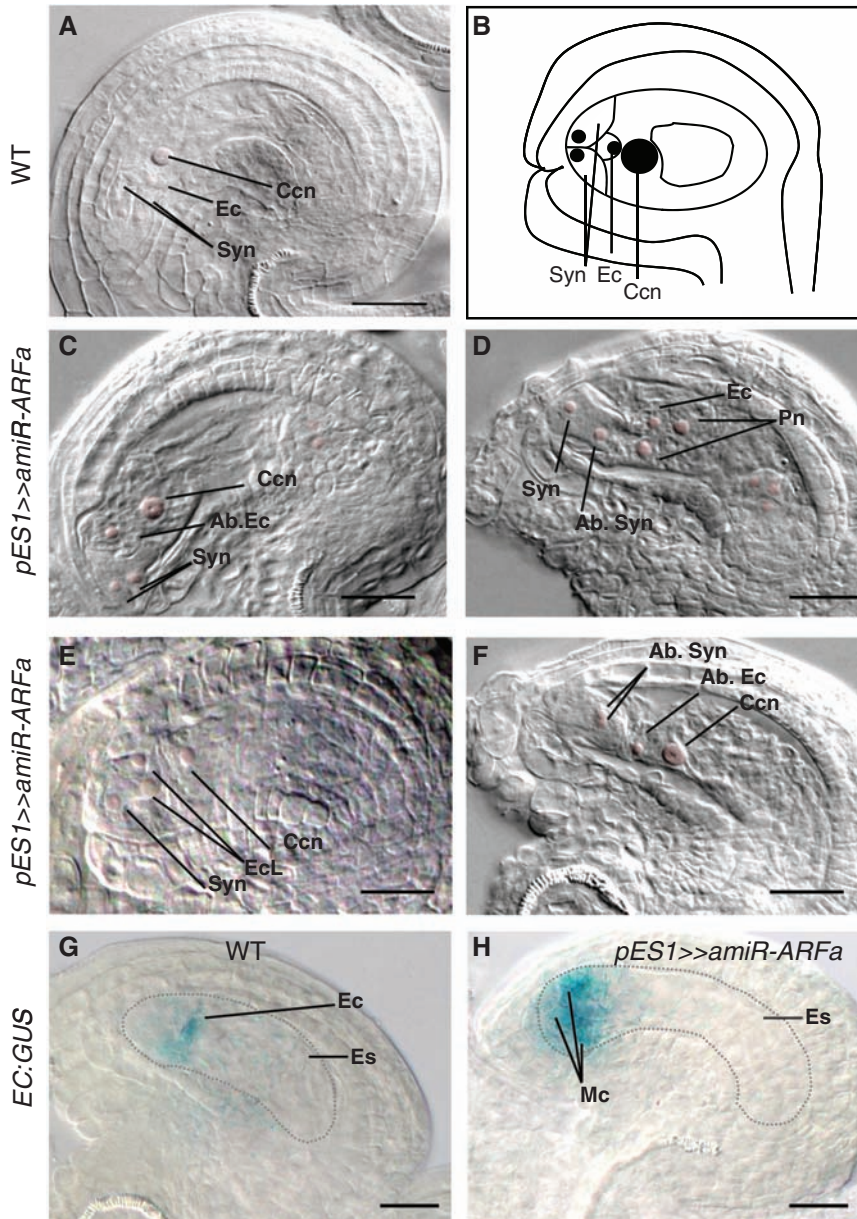

Fig. 2. When several ARF genes were down-regulated with an artificial miRNA expressed specifically in the embryo sac identity, defects in micropylar cells were observed. Scale bars, 25 μm. (**A**) DIC image of a wild-type (WT) embryo sac. Ccn, central cell nucleus; Ec, egg cell; and Syn, synergid. (**B**) Scheme of a WT female gametophyte. (**C**) Mature embryo sac showing an abnormal egg cell (Ab. Ec) with a centrally located nucleus. (**D**) Embryo sac showing unfused polar nuclei (Pn) and an abnormal synergid (Ab. Syn) cell, with a nucleus located toward the chalazal end of the embryo sac. (**E**) Embryo sac exhibiting two egglike cells. EcL, egg cell–like cell. (**F**) Embryo sac showing three cells morphologically similar to egg cells. (**G**) Expression of an egg cell–specific marker in a WT embryo sac. The developing embryo sac (Es) is delineated by a dashed line. (**H**) Expression of an egg cell–specific marker in all three micropylar cells of an ARF–down-regulated embryo sac. Mc, micropylar cell.

replaced with egg cell identity (Fig. 2, E and F). Markers for the central cell [pMEA-GUS (*6*)] and the antipodal cells [pAt1g36340-GUS (*7*)] were also tested in transgenic embryo sacs; however, GUS-staining patterns for these markers were similar in both phenotypically wild-type and abnormal embryo sacs (fig. S2, C and D, and table S3). Importantly, we observed no abnormalities in nuclear positioning at earlier stages of embryo sac development, and the overall positioning of nuclei at maturity was similar to that of wild-type embryo sacs (Fig. 2 and fig. S3). Therefore, it appears that auxin may not regulate nuclear positioning during embryo sac development but instead regulates cell fate specification at cellularization.

Auxin efflux and biosynthesis in developing female gametophytes. In order to determine the origin of the discrete auxin maxima observed, the expression of different auxin efflux facilitators (PINs) was studied in the developing embryo sac. Plants carrying fusions of *PIN1*, *PIN2*, *PIN3*, *PIN4*, and *PIN7* to GFP were used to study *PIN* expression in wild-type female gametophytes. No *PIN* expression was observed in the female gametophyte, but *PIN1* was expressed in the nucellus until the FG1 stage (fig. S4, A to C). The pattern of localization of *PIN1* suggests that auxin flux may occur in the nucellus, establishing an auxin maximum at the distal tip during the earliest stages of embryo sac development (fig. S4D). Later in development, *PIN1* expression was not observed in the gametophyte or the immediately adjacent sporophytic ovule tissues (fig. S4E).

YUCCA (*YUC*) genes encode key enzymes in auxin biosynthesis (*17–19*), and transgenic plants carrying *YUC::GUS* constructs (*17, 18*) showed that *YUC1* and *YUC2* expression overlapped with the auxin response signal in the ovules during megagametogenesis (Figs. 1 and 3). For both genes, *YUC* expression appears first at the micropylar region of the nucellus outside the embryo

sac at FG1 and then localizes to the micropylar pole of the gametophyte from FG2 through the later stages, while being undetectable in the nucellus (Fig. 3). This suggests that auxin might be synthesized initially at the nucellus and subsequently at the micropylar pole of the embryo sac during early embryo sac development, by at least these *YUC* genes.

To distort the polarized distribution of auxin observed in the embryo sac toward higher auxin levels, we expressed *YUC1* in the whole megagametophyte with the *Op-LhG4* transactivation system (*16*). Because YUC1 expression was driven by *pES1* throughout developing embryo sacs from FG1 to FG7 (*20*), we predicted that auxin would be distributed throughout the developing embryo sac if YUC1 substrates were present in the embryo sac. As expected *YUC1*-overexpressed female gametophytes did not establish a discernible auxin gradient, and *DR5::GFP* activity was detected in the entire female gametophyte from stages FG1 to FG5 (Fig. 4A and fig. S5). F1 plants overexpressing *YUC1* in the embryo sacs had about 25% defective ovules as identified by embryo sacs with micropylar cells with abnormal polarities as well as unfused polar nuclei and collapsed embryo sacs (Fig. 4, B and C, and table S4). Furthermore, antipodal cells that did not degenerate were detected in 34 of out of 268 overexpressed-YUC ovules examined (Fig. 4J).

We examined expression of a synergid-specific marker [ET884 (*6*)] normally expressed in wild-type embryo sacs only in the synergid cells. In YUC-overexpressing embryo sacs, the synergid marker was expressed in multiple cells, including those normally specified as egg cell, central cell, and the antipodals at the chalazal pole of the embryo sac (Fig. 4, D to F, and table S5). Equally frequently, in the YUC-overexpressing embryo sacs, an egg cell–specific marker [ET119 (*6*)] was also detected in the antipodal cells (Fig. 4H and table S5). In some cases this marker was exclusively expressed at the chalazal pole of the em-

bryo sac, where the antipodal cells are usually located (Fig. 4I). It may be that, in these *YUC1*-overexpressing embryo sacs, the cell at the position of the WT egg cell has assumed synergid attributes (Fig. 4, C and F).

Markers for the central cell and the antipodal cells in YUC-overexpressing embryo sacs showed similar GUS staining patterns in both wild-type and YUC-overexpressing embryo sacs with the pMEA-GUS central cell marker (*6*), indicating that overall central cell identity is maintained (table S5). Thus, the central cell seems to be less responsive to changes in local auxin concentrations than other female gametophytic cells, although, as noted, some central cells did express synergid markers. In addition, after fertilization we detected isolated embryo sacs that lacked endosperm development and had a morphological structure resembling a zygote at the position of the central cell, suggesting that the central cell might have switched to an egg cell fate (Fig. 4L). In contrast, the antipodal-specific marker *pAt1g36340-GUS* (*20*) showed expression only in a small fraction of the expected *YUC*-overexpressing embryo sacs carrying the GUS reporter (~10%, table S5). These observations were consistent with the reduction in the characteristic cell death after maturity that typifies antipodal cells.

We also ascertained whether the extra synergid-like cells observed in *YUC*-overexpressing embryo sacs interfered with normal pollen tube growth. When *YUC1*-overexpressing pistils were pollinated with wild-type pollen, two pollen tubes approaching and entering the female gametophyte were detected in 44 ovules out of 428 examined, of which 107 were predicted to contain embryo sacs carrying the two transgenes required to overexpress *YUC1*. By comparison, only 0.5% of wild-type ovules had more than one pollen tube enter the female gametophyte (*21*). These observations show that high auxin levels throughout the embryo sac alters cell identities, resulting in the conversion of chalazal cell identities to micropylar

Fig. 3. Expression of *YUCCA* genes in transgenic plants carrying *YUC1::GUS* and *YUC2::GUS* constructs suggests a role for auxin biosynthesis in gametophyte development. (**A** to **F**) Expression of *YUC1* (A to C) and *YUC2* (D to F) in wild-type embryo sacs. Scale bars, 25 μm. (A) *YUC1* expression in the nucellus at FG1 stage. (B) *YUC1* expression at the micropylar end of the embryo sac at stage FG3. (C) *YUC1* expression at the micropylar end of the embryo sac at stage FG4. (D) *YUC2* expression in the nucellus at FG1 stage. (E) *YUC2* expression at the micropylar end of the embryo sac at stage FG3. (F) *YUC2* expression at the micropylar end of the embryo sac at stage FG4.
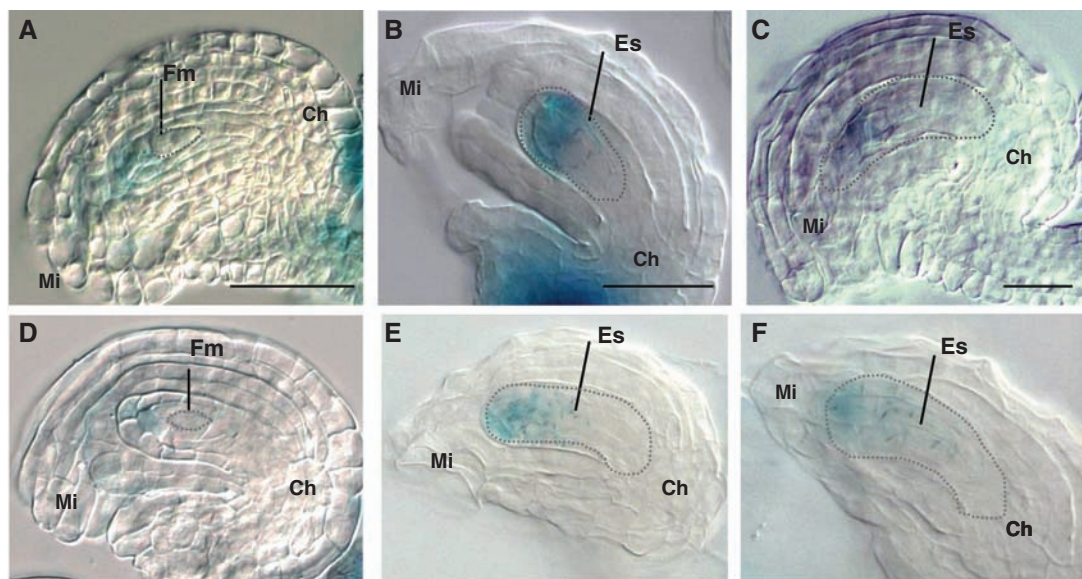
cell identities. As with the ARF–down-regulation experiments, we observed no abnormalities in nuclear positioning during embryo development arising from YUC1 overexpression (fig. S5), further confirming that nuclear positions within the syncitium are insensitive to auxin.

Auxin signaling and embryo sac development. We then examined mutants in auxin signaling for defects in cell specification. The *tir1 afb1 afb2 afb3* quadruple mutants have mutations in four genes of the *TIR* auxin receptor family and a significantly attenuated auxin response (*22*). From a total of 399 *tir1-1 afb1-1 afb2-1 afb3-1* embryo sacs examined, 82 showed defects in egg cell and synergid morphology, whereas 26 aborted at the 1 nuclear FG1 stage. The defective embryo sacs contained an additional egg cell–like cell replacing one of the two synergids, suggesting a switch of synergid to egg-cell fate (fig. S7A). We confirmed that at least some of these egg cell–like cells can function as gametic egg cells that form zygotelike structures after fertilization. By using embryonic markers introduced through the pollen, we demonstrated that the fertilized embryo sacs

contain two embryos, together with an absence of fertilized endosperm, indicating that the two sperm cells have fertilized two egg cells (fig. S7, B and C).

Models for patterning of the female gametophyte in *Arabidopsis* by auxin. Thus, our results suggest that cell-type specification arises from the positional information conferred by the distance of the different nuclei from a micropylar auxin source in the syncitial embryo sac. The early auxin flux in the nucellus, as indicated by the location of PIN1 expression, might be involved in establishing an initial sporophtyic auxin source, which could then provide the trigger for events establishing gametophyte patterning. The trigger could be auxin itself or another patterning factor that is generated within the nucellus at that location. In either case, we can consider two alternative models for the subsequent events. In one model, the sporophytic signal leads to auxin sources specified within the gametophyte at the micropylar pole that result in a gradient of auxin along the micropylar-chalazal axis (Fig. 5, A to C). The outcome is the graded specification of

different cell types, with the highest auxin concentrations specifying synergids, followed by egg cells, and the cells receiving the lowest amount of auxin developing into antipodal cells (Fig. 5D). In this model, all cells in the embryo sac might have the competence to differentiate into any of the different cell types composing the embryo sac, but the gradient of auxin directs the fate of each of the cells along the female gametophyte according to position. The positioning is determined by nuclear migration, which does not appear to be auxin-dependent, but may use other mechanisms (*8*). This proposed function of auxin in the embryo sac implies that it acts as a morphogen, that is, a source-derived gradient directing a concentration-dependent specification of different cell types, a concept for which support has been found in sporophytic root development (*23*, *24*). One difference is that the gametophytic auxin appears to be synthesized locally and in this respect resembles more closely the classical morphogen systems in animals.

Alternatively, gametophytic auxin might not be the primary instructive signal but might instead

Fig. 4. Phenotype of *YUC1*-overexpressing embryo sacs and two alternative models for auxin-dependent cell specification in the female gametophyte. Scale bars, 25 μm. (**A**) DR5::GFP activity is localized in the whole embryo sac (Es) of *YUC1*-overexpressing embryo sacs at FG5. (**B**) Polarized DR5::GFP activity detected in a WT embryo sac at FG5. Ccn, central cell nucleus; Syn, synergid cells; and Syn LC, synergid-like cell. (**C**) A *YUC1*-overexpressing embryo sac with a synergid-like cell at a position in which the egg cell is usually located. (**D**) WT embryo sac showing the expression of a specific synergid marker. Ch, chalazal end of the embryo sac, and mi, micropylar end of the embryo sac. (**E**) Expression of the synergid marker in a *YUC1*-overexpressing embryo sac shows signal in the positions of both the synergid cells and the antipodal cells. (**F**) Expression of the synergid marker is detected in cells at the positions of synergids, egg cell, and central cell in a *YUC1*-overexpressing embryo sac. (**G**) Wild-type embryo sac showing the expression of an egg cell (E.C)–specific marker. (**H**) *YUC1*-overexpressing embryo sac exhibiting expression of the egg cell marker in a cell at the position of the egg cell and a cell at the antipodal position. (**I**) *YUC1*-overexpressing embryo sac showing expression of the egg cell marker only in a cell at the antipodal position. (**J**) Mature and unfertilized *YUC1*-overexpressing embryo sac from an emasculated flower showing surviving antipodal cells (S Ant) 2 days after emasculation. (**K**) Two pollen tubes (Pt) enter the micropyle of a *YUC1*-overexpressing embryo sac and continue to grow within the embryo sac. F,

funiculus. (**L**) Fertilized *YUC1*-overexpressing embryo sac showing no endosperm development and a structure that morphologically resembles a zygote at the position of the central cell. EcL, egg cell–like cell; Z, zygote, and ZL, zygotelike cell.
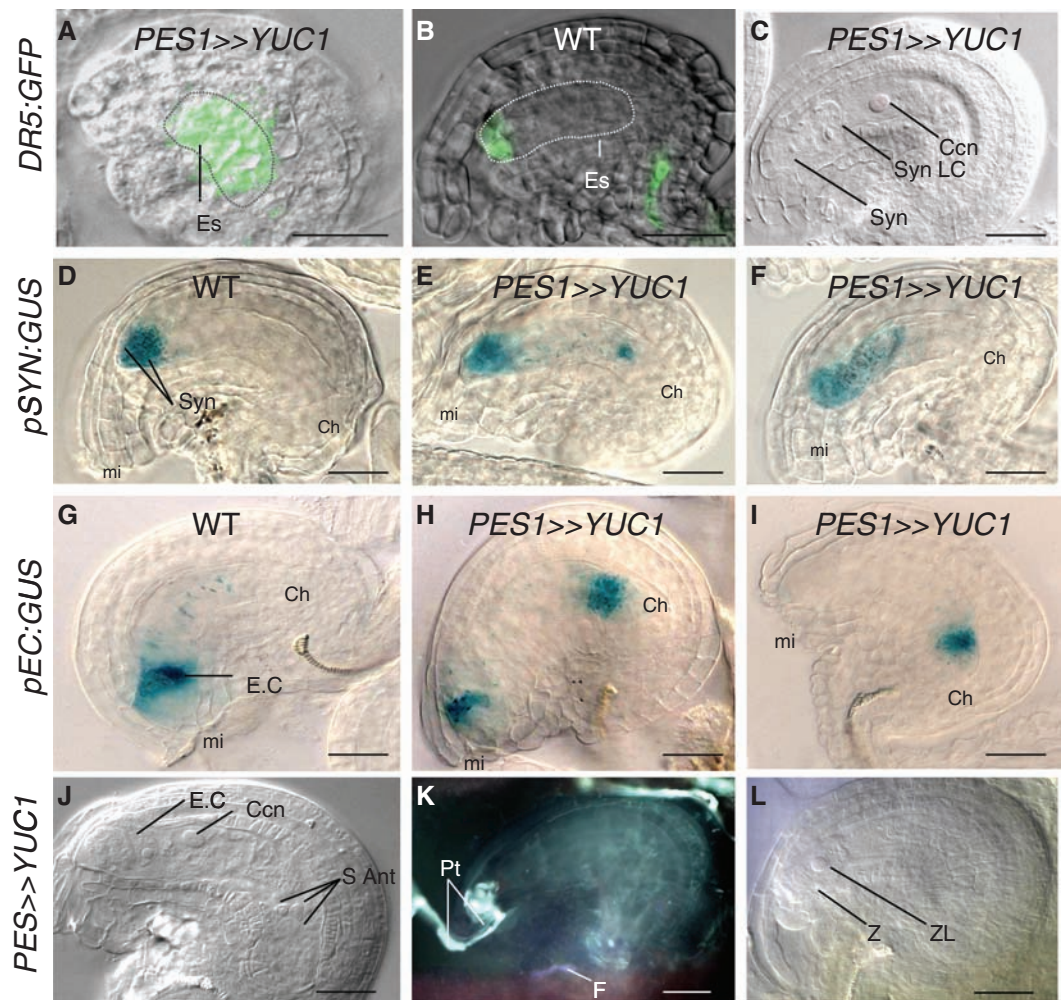
act downstream of an undiscovered patterning factor "X" acting at the micropylar pole, which then induces *YUC* expression in the micropylar nuclei, resulting in the observed asymmetric auxin distribution (Fig. 5, E to H). In this model, high auxin might promote synergid cell fate, whereas egg-cell fate might be the consequence of lower levels of X that then result in lower auxin (Fig. 5H). The central cell and antipodals could then be specified by secondary auxin-independent mechanisms. The observation that central cell specification appears to be less susceptible to auxin levels than the other cells is consistent with the latter model. However, the relative stability of central cell fate to auxin perturbations can also be reconciled with the auxin as morphogen model. Because the central cell nucleus normally results from the fusion of two polar nuclei initially located at opposite sides of the female gametophyte, and these nuclei are hypothesized to be exposed to quite different auxin concentrations that are nonetheless intermediate between the egg apparatus and antipodals, specification of central cells might occur within a broader concentration range. Cells at this position are in fact capable of assuming synergid or egg cell attributes in high auxin (Fig. 4, F and L). Further studies will be needed to discriminate between these alternative models for patterning.

The maintenance of an auxin gradient within the syncitial embryo sac is unexpected. The localization of YUC gene expression, as well as the auxin GFP reporter, might be explained by the observation that the embryo sac syncitium is partitioned into cytoplasmic domains (*25*, *26*); such partitioning may restrict translation of messenger RNAs to the domain containing the nucleus where the transcript originated. However, auxin has a diffusion constant two orders of magnitude greater than GFP and is likely to diffuse rapidly even with cytoplasmic partitioning. Thus, it is probable that other mechanisms maintain a polarized auxin distribution, such as non-PIN auxin carriers or through the inactivation of auxin by conjugation or degradation at the chalazal pole.

Implications. This study provides support for the modular hypothesis of female gametophyte evolution (*1*, *2*, *27*). If the seven-cell/eight-nucleate *Polygonum*-type embryo sac that characterize the majority of the angiosperms is the result of a four-nuclei/cell module duplication, then cells in each of the modules might have conserved the capacity to differentiate into egg cells and synergids despite the loss of these functions at time of divergence of the basal angiosperm lineages >120 million years ago (*2*). Our observation that synergid and egg cell attributes can be generated at both poles of the embryo sac is consistent with this prediction. We hypothesize that, after the initial duplication, the potential egg apparatus located at the chalazal pole would be within a field of low auxin because of its distal position relative to the micropylar auxin source, leading to acquisition of a default cell fate as antipodal cells as a side effect (*2*). This study may also provide

insights into the variation observed among angiosperm embryo sacs. Although the eight nuclear *Polygonum*-type embryo sac predominates, a wide variety of embryo sacs with 4 to 16 nuclei have been documented; yet in all such cases a unique egg cell develops and results in monozygotic seed when fertilized, although the number of haploid nuclei within the endosperm varies (*28*, *29*). This can be explained if the egg apparatus is always specified by its proximal location to the micropylar auxin source, which itself may be initially specified by the sporophyte. The formation of a single embryo in fertilized seeds, combined with variation in maternal genotype and ploidy of endosperm tissue, may determine fitness by affecting both the paternal genome dosage and the effects of imprinting that control seed size, as well as the relatedness between the endosperm and embryo (*29*).

Lastly, it is interesting to consider our results within the framework of the ancestral function of auxin in gametophyte patterning. Analyses of extant land plants and paleobotanical evidence indicate that the reduced female gametophyte of angiosperms is derived from an ancestral, complex, free-living gametophyte (*30*). Although little is known about the genetic basis of pattern formation of extant land plants with complex gametophytes, pharmacological experiments implicate that auxin is an important factor (*31*), despite evidence that polar auxin transport may be restricted to the sporophyte in several mosses studied (*31*, *32*). We hypothesize that localized auxin synthesis, along with the induction of sequential sources combined with auxin degradation/conjugation, rather than PIN-mediated transport might have been more important in establishing the patterning of lower plant gametophytes. Given their evolutionary history, it is likely that genetic programs patterning the female gametophytes of angiosperms were inherited from those patterning the complex three-dimensional tissues of ancestral gametophytes.
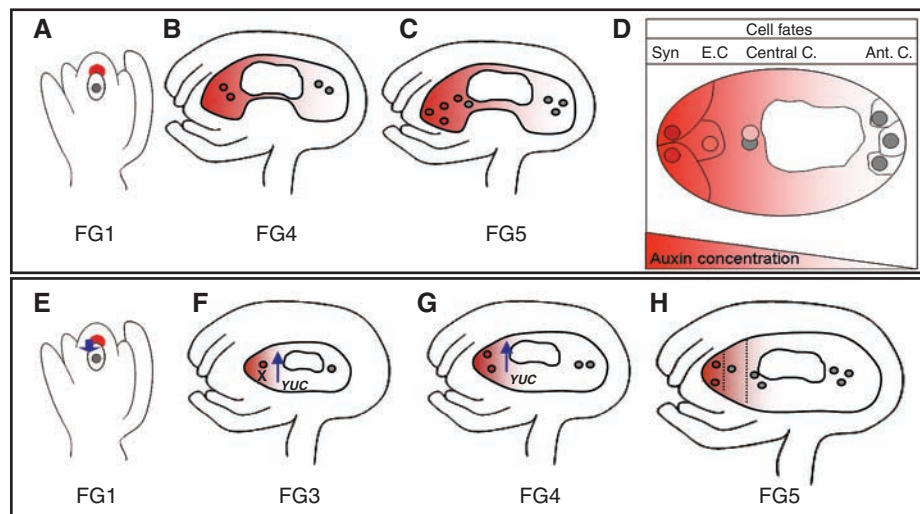

Fig. 5. Models for patterning of the female gametophyte. (**A** to **D**) Auxin gradient model for patterning. (A) At FG1 stage, the auxin source is sporophytic and is derived from the nucellus. (B) Subsequently, a secondary auxin source is specified locally within the gametophyte at the micropylar pole. (C) Auxin gradient with a maximum at the micropylar pole of the embryo sac. (D) Auxin concentration determines cell fates, with the highest auxin concentrations specifying synergids (Syn), followed by egg cells (E.C.), and the lowest auxin resulting in antipodal (Ant.) cells. Central C., central cell. (**E** to **H**) Model for patterning by a nonauxin molecule acting through auxin. (E) Nucellus generates a signal (block arrow), which might originate from the auxin source. (F) This signal induces a factor X at the micropylar pole, which then induces auxin synthesis by activating *YUCCA* gene expression in the nucleus located at that pole. (G) Continued synthesis of auxin at micropylar pole. (H) Two of the micropylar nuclei are in the high auxin zone and differentiate into synergids, whereas the third micropylar nucleus in lower auxin differentiates into the egg cell. In this model, the central cell and antipodal cell fates could be specified by auxin-dependent or auxin-independent mechanisms.

References and Notes
1. M. W. Frohlich, M. W. Chase, *Nature* **450**, 1184 (2007).
2. J. H. Williams, W. E. Friedman, *Plant Cell* **16**, S119 (2004).
3. C. A. Christensen, E. J. King, J. R. Jordan, G. N. Drews, *Sex. Plant Reprod.* **10**, 49 (1997).
4. C. A. Christensen, S. Subramanian, G. N. Drews, *Dev. Biol.* **202**, 136 (1998).
5. J. M. Moore, J. P. V. Calzada, W. Gagliano, U. Grossniklaus, *Cold Spring Harbor Symp. Quant. Biol.* **62**, 35 (1997).
6. R. Gross-Hardt *et al.*, *PLoS Biol.* **5**, e47 (2007).
7. G. C. Pagnussat *et al.*, *Development* **132**, 603 (2005).
8. G. C. Pagnussat, H. J. Yu, V. Sundaresan, *Plant Cell* **19**, 3578 (2007).
9. M. M. S. Evans, *Plant Cell* **19**, 46 (2007).
10. D. Umulis, M. B. O'Connor, H. G. Othmer, *Curr. Top. Dev. Biol.* **81**, 65 (2008).
11. E. Benkova *et al.*, *Cell* **115**, 591 (2003).
12. J. Friml *et al.*, *Nature* **426**, 147 (2003).
13. J. Mattsson, W. Ckurshumova, T. Berleth, *Plant Physiol.* **131**, 1327 (2003).
14. S. Sabatini *et al.*, *Cell* **99**, 463 (1999).
15. T. Ulmasov, J. Murfett, G. Hagen, T. J. Guilfoyle, *Plant Cell* **9**, 1963 (1997).
16. Materials and methods are available as supporting material on *Science* Online.

17. Y. Cheng, X. H. Dai, Y. D. Zhao, *Genes Dev.* **20**, 1790 (2006).
18. Y. Cheng, X. H. Dai, Y. D. Zhao, *Plant Cell* **19**, 2430 (2007).
19. Y. Zhao *et al.*, *Science* **291**, 306 (2001).
20. H. J. Yu, P. Hogan, V. Sundaresan, *Plant Physiol.* **139**, 1853 (2005).
21. N. Huck, J. M. Moore, M. Federer, U. Grossniklaus, *Development* **130**, 2149 (2003).
22. N. Dharmasiri *et al.*, *Dev. Cell* **9**, 109 (2005).
23. O. Leyser, *Cell* **121**, 819 (2005).
24. C. Galinha *et al.*, *Nature* **449**, 1053 (2007).
25. R. C. Brown, B. C. Lemmon, *EMSA Bull* **22**, 48 (1992).
26. R. C. Brown, B. C. Lemmon, *Protoplasma* **165**, 155 (1991).
27. W. E. Friedman, J. H. Williams, *Evolution* **57**, 216 (2003).
28. V. Brukhin, M. D. Curtis, U. Grossniklaus, *Curr. Sci.* **89**, 1844 (2005).
29. W. E. Friedman, E. N. Madrid, J. H. Williams, *Int. J. Plant Sci.* **169**, 79 (2008).
30. P. Kenrick, P. R. Crane, *The Origin and Early Diversification of Land Plants: A Cladistic Study* (Smithsonian Series in Comparative Evolutionary Biology, Smithsonian Institution, Washington, DC, 1997).
31. T. J. Cooke, D. Poli, A. E. Sztein, J. D. Cohen, *Plant Mol. Biol.* **49**, 319 (2002).
32. T. Fujita *et al.*, *Evol. Dev.* **10**, 176 (2008).
33. We thank U. Grossniklaus for providing the cell-specific marker lines used in this study; B. Sheres, J. Friml, and M. Tasaka for providing plants carrying PIN::GFP fusions; Y. Zhao for providing YUC::GUS reporter lines and YUC1 cDNA; N. Dharmasiri for seeds of the *tir1afb* quadruple

Extending Universal Nodal Excitations Optimizes Superconductivity in Bi$_2$Sr$_2$CaCu$_2$O$_{8+\delta}$

Aakash Pushp,[1,2]* Colin V. Parker,[1]* Abhay N. Pasupathy,[1]† Kenjiro K. Gomes,[1]‡ Shimpei Ono,[3] Jinsheng Wen,[4] Zhijun Xu,[4] Genda Gu,[4] Ali Yazdani[1]§

Understanding the mechanism by which *d* wave superconductivity in the cuprates emerges and is optimized by doping the Mott insulator is one of the major outstanding problems in condensed-matter physics. Our high-resolution scanning tunneling microscopy measurements of the high–transition temperature (T_c) superconductor Bi$_2$Sr$_2$CaCu$_2$O$_{8+\delta}$ show that samples with different T_c values in the low doping regime follow a remarkably universal *d* wave low-energy excitation spectrum, indicating a doping-independent nodal gap. We demonstrate that T_c instead correlates with the fraction of the Fermi surface over which the samples exhibit the universal spectrum. Optimal T_c is achieved when all parts of the Fermi surface follow this universal behavior. Increasing the temperature above T_c turns the universal spectrum into an arc of gapless excitations, whereas overdoping breaks down the universal nodal behavior.

Central to the current debate on the mechanism underlying high-temperature superconductivity is the question of whether pairing strength in the cuprates is diminished as these systems approach the Mott insulator limit with reduced hole density. The panoply of physical phenomena in lightly doped cuprates near the Mott state uncovered over the last two decades—from observation of the pseudogap behavior (*1*, *2*) to fluctuating superconductivity (*3*) above the transition temperature (T_c) to the

possibility of other competing orders (*4*–*6*)—have made addressing this question challenging. In a simple *d* wave superconductor, a single energy scale suffices to completely describe the excitation spectrum, the associated pairing energy gap (including its angular and temperature dependence), as well as the T_c of the sample. In the underdoped cuprates, however, there is increasing evidence (*7*–*12*) that a single energy scale is insufficient to describe the anisotropy of the energy gap because different behavior is seen near the node (45° to the Cu–O bond direction) and the anti-node (along the Cu–O bond direction). The temperature evolution of the spectroscopic measurements has also shown a dichotomy between nodal and anti-nodal gaps, showing different temperature dependence (*8*, *10*, *13*). Theoretical proposals for addressing these phenomena include those based on phase fluctuations of preformed pairs (*14*–*16*), incipient order (*5*), breakup of the Fermi surface due to umklapp scattering (*17*), and incoherence of anti-nodal quasi-particles (*18*). Although it is clear that the gap near the anti-node increases as one ap-

proaches the Mott insulator (*19*), the behavior of the gap near the node still remains debated, with different measurements showing both increasing (*19*–*21*) and decreasing (*7*, *8*, *22*) trends with underdoping. Whether pairing gaps associated with nodal excitations track the samples' T_c, as expected for simple *d* wave superconductors, is an unresolved question that deeply affects our understanding of superconductivity in the cuprates. The answer to this question can determine if the pairing is derived from the strong electronic correlations of the Mott state and can identify the mechanism by which *d* wave superconductivity is optimized in proximity to an insulating ground state.

To elucidate the nature of the nodal and anti-nodal gaps as a function of doping and temperature, we performed atomically resolved scanning tunneling microscopy (STM) measurements on Bi$_2$Sr$_2$CaCu$_2$O$_{8+\delta}$ (BSCCO) in the doping range of $0.07 < x < 0.24$ (where x is the nominal hole doping) and a temperature range from 5 to 120 K. Spectroscopic measurements in our home-built scanning tunneling microscope can be performed with sub–millielectron volt energy resolution on the same atomic location as a function of temperature (*9*, *23*). Although STM spectroscopy does not have intrinsic angular resolution, information about the nodal gap can be obtained from the spectrum near the Fermi energy, whereas the anti-nodal excitations occur at higher energy. We can use this information to extract the behavior of the nodal gap.

The complexity of the excitation spectrum in underdoped BSCCO samples (Fig. 1A) is seen in lattice-tracking spectroscopy (*9*, *23*) measurements, in which we track the temperature evolution of tunneling spectra at a given atomic location. This spectrum (typical for this sample) shows a higher energy gap, Δ_0, (black arrow in Fig. 1A), a smaller "kink" within the higher energy gap (red arrow in Fig. 1A), and an overall background, all of which are position dependent. Δ_0, determined by the maximum conductance on the positive side, shows strong spatial inhomogeneity (*24*, *25*) on the sample (Fig. 1C). The spatial average of the higher energy gap compares well with angle-resolved

[1]Joseph Henry Laboratories and Department of Physics, Princeton University, Princeton, NJ 08544, USA. [2]Department of Physics, University of Illinois at Urbana-Champaign, Urbana, IL 61801, USA. [3]Central Research Institute of Electric Power Industry, Komae, Tokyo 201-8511, Japan. [4]Condensed Matter Physics and Materials Science, Brookhaven National Laboratory (BNL), Upton, NY 11973, USA.

*These authors contributed equally to this work.
†Present address: Department of Physics, Columbia University, New York, NY 10027, USA.
‡Present address: Department of Physics, Stanford University, Stanford, CA 94305, USA.
§To whom correspondence should be addressed. E-mail: yazdani@princeton.edu